Chapter 3

“Iron doped titania/multiwalled carbon nanotube nanocomposite: a robust electrocatalyst for hydrogen evolution reaction in aqueous acidic medium”

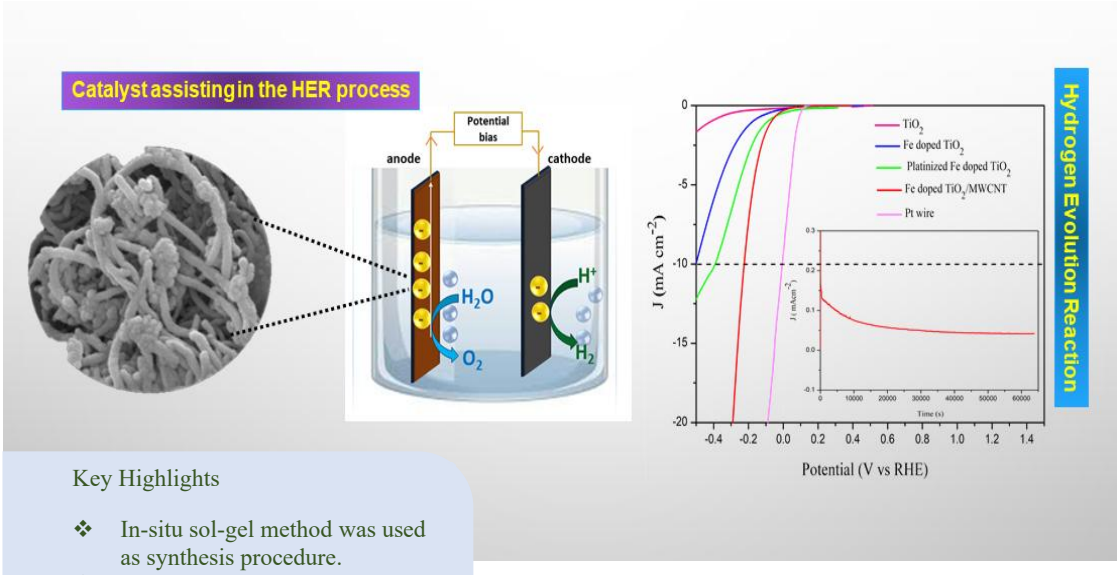

Key Highlights

- In-situ sol-gel method was used as synthesis procedure.
- 221 mV overpotential was required
- The catalyst is quite stable in 0.5 M H_2SO_4 upto 17.7 hr
- Optimum catalytic activity was obtained with 0.50 wt% of MWCNT content.

3.1 Introduction

In the contemporary world energy and the environment are the two key concerns for the development of an environmentally balanced system. Since hydrogen is the major substitute for fossil fuels the research community tried to find earth-abundant electrocatalysts that are synthesized via a green method. Non-noble metals (Ni, Co, Mo, Fe) and their metal oxides, sulfides, selenides, and phosphides are being studied for their possibilities as cathodic electrocatalysts [1-4]. However, apart from the oxides, the synthesis procedure of most of the active catalysts is complex and often involves use of the hazardous chemicals. TiO_2 is a very low-cost and environmentally friendly metal oxide. TiO_2 nanoparticle-supported metal catalysts offer high stability due to its mesoporous structure [5]. Both metallic and non-metallic element doping can shorten the band gap of TiO_2 (3.2 eV), thereby impacting both their photocatalytic and electrocatalytic performance in a positive way [6]. Moreover, doping can also increase metal-support interactions that is responsible for the improvement of the electrocatalytic properties [7]. Among different dopant elements Fe, in particular, is highly suitable because of its low cost, low toxicity, and easy availability. Khan *et al.* hydrothermally prepared Fe^{3+} doped TiO_2 for photocatalytic hydrogen production using visible light [8]. Danilov *et al.* synthesized Fe/TiO_2 composite to carry out HER in alkaline medium [9]. They synthesized the composite coating by electrodeposition and were able to achieve remarkable HER activity at 470 mV at 250 mA cm^{-2}. In this catalyst, titania increases both the surface area as well as the number of active sites. The catalytic activity was also reinforced by the manifestation of the redox couple containing Ti ($TiO_2 \rightleftarrows Ti_2O_3 \rightleftarrows TiOOH$). Despite such beneficial chemical properties of titania its application is often restricted because of its lower electrical conductivity [10].

This part of the thesis is published in:

Lahkar, S., Ahmed, S., Mohan, K., Saikia, P., Das, J.P., Puzari, P., and Dolui, S.K. Iron doped titania/multiwalled carbon nanotube nanocomposite: A robust electrocatalyst for hydrogen evolution reaction in aqueous acidic medium. *Electrochimica Acta*, *407*:139921, 2022.

Literature review also reveals that the exploration of Fe as HER catalyst has not been as elaborate as other transition metals like Mo and Ni. One of the reasons is that 3d series of transition metals are not stable in acids, however, HER is preferred in acidic medium as plenty of protons are available in the electrolyte to facilitate hydrogen generation [11].

The limitations of both TiO_2 and Fe nanoparticles concerning lower electrical conductivity and acidic corrosivity can be overcome to a great extent by using carbon-based nanomaterials (like graphene, carbon aerogel, amorphous carbon, multiwalled carbon nanotubes (MWCNTs), etc.). Carbon materials show excellent electrical conductivity and have high surface areas. Hence, can act as excellent support material. These properties have already drawn the attention of researchers towards their use in photocatalytic degradation of organic pollutants [12], wastewater treatment [13], photoinactivation of some bacteria [14], catalytic oxidation [15], etc. Carbon nanomaterials are also highly resistant to acidic corrosion caused by the electrolyte, thus MWCNTs can increase the longevity of the catalyst. Lin *et al*. reported direct growth of tungsten carbide and tungsten disulphide on carbon nanotubes (CNTs) by annellation that showed suitable use in HER with overpotential value of 489 mV and 684 mV respectively at 10 mA cm^{-2} [16]. Cao et al. used MWCNT as a conductive support for poor intrinsic conductive MoS_2. They found that strong electronic coupling between the MWCNTs and MoS_2 greatly improves the catalytic efficiency and also the stability of HER [17]. Deng *et al.* used Fe encapsulated into nitrogen-doped CNTs as HER catalyst in acidic electrolyte to obtain encouraging results [18]. Tavakkoli *et al.* synthesized single shell carbon-encapsulated Fe nanoparticles (SCEINs) decorated on single-walled carbon nanotubes (SWNTs) with catalytic property comparable to that of Pt [19]. Dai *et al*. reported MWCNT-TiO_2 nanocomposite synthesized *via* hydrothermal process. The catalyst showed a very good response towards photocatalytic HER with 3.8% quantum efficiency along with good stability [20].

From the extensive study of literature, our conjecture is that the overall synergetic effect of all the three components, i.e., Fe, TiO_2 and MWCNT may lead to good catalytic activity for HER with better conductivity, catalytic support and corrosion resistance. The present work proposes the application of a Pt-free material, Fe doped TiO_2/MWCNT nanocomposite, as an electrocatalyst with superior catalytic activity and stability for HER in acidic medium. Role of Fe doped TiO_2/MWCNT

composite has earlier been studied by Koli and his research group in photoinactivation of bacteria [14]. But to the best of our knowledge, its potential for electrocatalytic activity has not been explored yet. A sol-gel method is used as mentioned by Koli *et al.* with a slight modification to synthesize Fe-doped TiO_2/MWCNT nanocomposite. The structural properties of the catalyst are investigated by XRD, FTIR, SEM, EDX, and TEM. Performance of the electrocatalyst towards HER is evaluated by analyzing its polarization curve and Tafel plot. Durability and stability of the catalyst are assessed by chronoamperometry and cyclic voltammetry (CV) tests, and a plausible HER mechanism is also addressed.

3.2 Materials and methods

3.2.1 Materials

All the chemicals including MWCNT, titanium tetraisopropoxide (TTIP), iron (III) nitrate nonahydrate ($Fe(NO_3)_3.9H_2O$), sodium dodecylbenzenesulfonate (NaDDBS), ammonia solution (25%,), chloroplatinic acid (H_2PtCl_6), sodium borohydride ($NaBH_4$), sodium hydroxide (NaOH), ethanol, acetic acid, sulphuric acid (H_2SO_4) and nitric acid (HNO_3) purchased from Sigma-Aldrich were analytical reagent grade purity and were directly used.

3.2.2 Methods

3.2.2.1 Acid functionalization MWCNTs

Since the catalyst synthesis procedure was carried out in the solution (water) phase, first, we functionalize MWCNT. For -COOH functionalization reflux of MWCNT was carried out with a mixture of H_2SO_4:HNO_3 in 3:1 (v/v) ratio for 4h at 90°C. After that, the sample mixture was cooled down to room temperature, centrifuged and washed with distilled water for several times to neutralise the pH. The final product was dried at 80°C to generate acid-functionalized MWCNTs [14].

Varying contents of acid-functionalized MWCNTs: 0.35, 0.50, and 0.65 wt% were ultrasonicated in aqueous solutions of 0.5 weight% NaDDBS overnight to get a homogeneous dispersion for use in the synthesis of the nanocomposite in the next section.

3.2.2.2 Synthesis of Fe doped TiO_2/MWCNT nanocomposite

Fe doped TiO_2/MWCNT nanocomposite was synthesized from the titania precursor TTIP and a Fe source $Fe(NO_3)_3.9H_2O$ by sol–gel technique. 0.03 wt% of $Fe(NO_3)_3.9H_2O$ was dissolved in 1.1 mL H_2O (solution A). In another beaker 0.5 mL TTIP was mixed with 6 mL ethanol and 3 mL of 0.6 M HNO_3, and stirred for 30 min till a clear solution (solution B) was obtained. Afterward, solution B was poured into solution A dropwise under continuous stirring over a period of 0.5 h. Following that, the prepared mixture of solution A and solution B was added dropwise into the 0.35 wt% MWCNT suspension under vigorous stirring. The new mixture was further stirred at a temperature of 60°C for 5 h. Thereafter, dilute ammonia solution was added dropwise to adjust the pH of the overall sample solution to 10 in order to complete the hydrolysis of the titania precursor. The obtained precipitate was collected by centrifugation and then washed with ethanol and distilled water several times. It was then dried at 80°C for 12 h, followed by calcination in air at 450°C for 4 h. The whole process was repeated with 0.50 and 0.65 wt% MWCNT suspensions to obtain Fe doped TiO_2/MWCNT nanocomposites with varying MWCNT contents.

For comparative study, TiO_2, Fe doped TiO_2 and platinized Fe doped TiO_2 were also synthesized using the following synthesis procedures.

3.2.2.3 Synthesis of TiO_2

Anatase form of TiO_2 used in the experiment was synthesized by using the conventional hydrothermal method [21]. 2 mM titanium tetraisopropoxide (TTIP, 97%, Aldrich Chemical Co.) was added dropwise to the 150 mL mixture solution of ethanol and water. pH of the solution was maintained to be 0.7 by adding 0.5 M nitric acid. The solution was then stirred vigorously for 1 h to obtain a clear solution without precipitation. Following that the solution was transferred to a Teflon lined autoclave and hydrothermal reaction was carried out at 240^0C for 4 h. The colloidal suspension thus obtained was centrifuged to collect the precipitate and washed for several times with distilled water. The as obtained precipitate was then vacuum-dried and calcinated at 500^0C for 5 h. Pale yellow TiO_2 particles were obtained which was used for characterization.

3.2.2.4 Synthesis of Fe doped TiO_2

1 M TTIP was prepared in ethanol by continuous stirring for half an hour (solution A). 0.03 wt% of $Fe(NO_3)_3 \cdot 9H_2O$ was dissolved in the mixture of 12.7 mL CH_3CH_2OH, 16.1 mL CH_3COOH and 2.2 mL H_2O (solution B). Next, solution 'B' was slowly dropped onto solution 'A' over a period of half an hour. The final solution was stirred for ½ h more before transfering into a 100 mL Teflon-lined stainless-steel autoclave. The hydrothermal reaction was carried out at 180^0C for 24 h [22]. A powdered product was obtained after filtrating and washing with ethanol and distilled water several times and then dried at 80^0C. The dried sample was then calcined at 500^0C for ½ h. The obtained light yellow coloured Fe doped TiO_2 was used in the experiment.

3.2.2.5 Synthesis of platinized Fe doped TiO_2

Fe doped TiO_2 was platinized using a reducing reagent following a similar route as referred by Pan *et al.* with slight alterations [23]. Here, 50 mg of Fe doped TiO_2 was dispersed homogeneously in 10 mL distilled water. After that, 20 mM H_2PtCl_6 solution was added dropwise to the above dispersion with continuous stirring followed by addition of 10 mL of an aqueous solution of 50 mM $NaBH_4$ dropwise. The pH of the added $NaBH_4$ solution was maintained to be 12 by adding NaOH. The mixture solution was kept under constant stirring for 3 h at 55^0C. The precipitate was filtered and washed with distilled water to neutralize the pH. The resulting sample was dried in oven at 80^0C for 12 h.

3.2.3 Characterization and Measurements

The synthesized materials are characterized by XRD, FTIR, SEM, FESEM, TEM and EDX analysis. All the electrochemical measurements were performed on a Bio-Logic SP-150 potentiostat. The electrochemical behaviours of the samples were studied using a standard three electrodes cell compartment where Pt and standard calomel electrode (SCE) were used as the counter and the reference electrodes respectively. The working electrode was prepared by dispersing 6 mg of the synthesized electrocatalyst in 0.1 mL 0.5 wt% Nafion solution and coated onto the ~ 0.07 cm^2 surface area of glassy carbon electrode (GCE, radius 1.5 mm) and then naturally dried at room temperature. 0.5 M H_2SO_4 aqueous solution was used for all the electrical measurements.

3.3 Results and Discussion

3.3.1 XRD analyses.

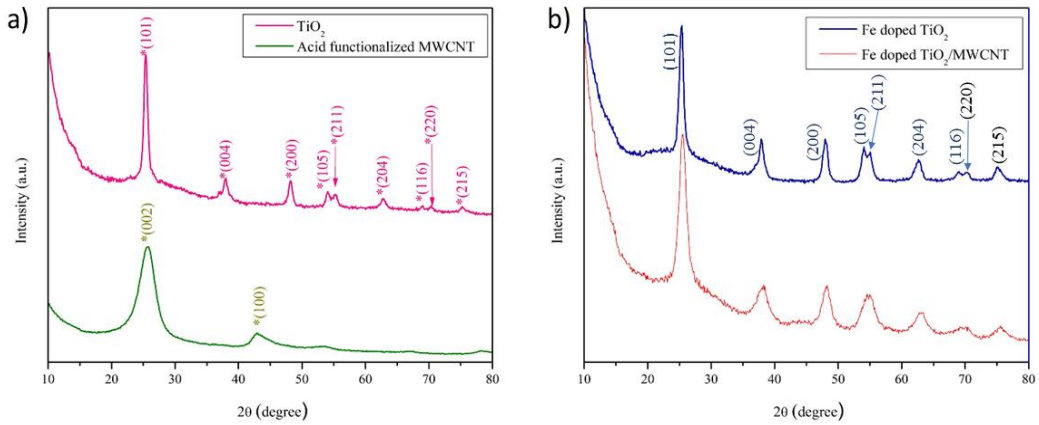

Figure 3.1 XRD patterns of (a) TiO_2 and acid functionalized MWCNT, (b) Fe doped TiO_2/MWCNT and Fe doped TiO_2

Crystallinity of the prepared samples were studied by XRD. Synthesized TiO_2 nanoparticles exhibit characteristic peaks at $2\theta = 25.43^{\circ}$, 37.76°, 48.14°, 53.95°, 55.07°, 62.76°, 68.96°, 70.26° and 75.15° which correspond to (101), (004), (200), (105), (211), (204), (116), (220) and (215) planes of anatase phase of titania respectively. However, no rutile peaks are identified **(Figure 3.1 (a))**. In case of acid-functionalized MWCNT **(Figure 3.1 (a))**, two significant peaks are observed, one at $2\theta = 25.43^{\circ}$ for (002) plane and another at $2\theta = 43.67^{\circ}$ for (100) plane. XRD pattern of Fe doped TiO_2/MWCNT represents the anatase phase TiO_2, with the (002) plane of MWCNT merging with (101) plane of the TiO_2. The intensity of the peak at $2\theta = 25.43^{\circ}$ becomes stronger due to this merger. A low concentration of Fe cannot change the crystal structure which remains intact. From **Figure 3.1 (a) and (b)**, it is observed that TiO_2, Fe doped TiO_2 and Fe doped TiO_2/MWCNT all show consistent peaks at the same positions. Both titania and iron doped titania particles display sharp crystalline peaks, however, in Fe doped TiO_2/MWCNT (**Figure 3.1 (b)**) the peaks get broadened which is indicative of nanoscale material formation and hence increasing surface area of the catalyst [24] and it is also confirmed through electrocatalytic active surface area (ECSA) calculation later. These significant criteria of the composite manifest in higher electrocatalytic activity towards HER.

3.3.2 FTIR analyses.

The functional groups present in acid functionalised MWCNT, Fe doped TiO_2 and Fe doped TiO_2/MWCNT composite were determined from FTIR spectroscopic analysis **(Figure 3.2)**. In the IR spectrum of acid functionalised MWCNTs, the absorption peak at 3429 cm^{-1} corresponds to O-H stretching mode and the one at 1633 cm^{-1} is due to C=O or C=C stretching mode [25,26]. The peak at 1043 cm^{-1} ascribes to the C–O stretching vibrations [25]. Acid pre-treatment of MWCNTs generates oxygen-containing groups that form intimate contact between MWCNTs and Fe doped TiO_2, leading to fine stability of the composites. The spectrum of Fe doped TiO_2 shows significant absorption peak for O-H stretching mode at 3434 cm^{-1} along with an absorption band at 1624 cm^{-1} that represents H-O-H bending vibration. These two peaks mainly come due to moisture adsorption on the material surface. A broad absorption peak at 784 cm^{-1} is characteristic of Ti-O-Ti bond vibration [27]. The IR spectrum of Fe doped TiO_2/MWCNT has absorption bands corresponding to O-H vibration band along with stretching vibration frequencies of Ti-O-Ti at 3434 cm^{-1} and at 618 cm^{-1} respectively. A low intensity peak at 1381 cm^{-1} due to Ti-O-C bond confirms the covalent interaction of Fe doped TiO_2 particles with the MWCNTs [26].

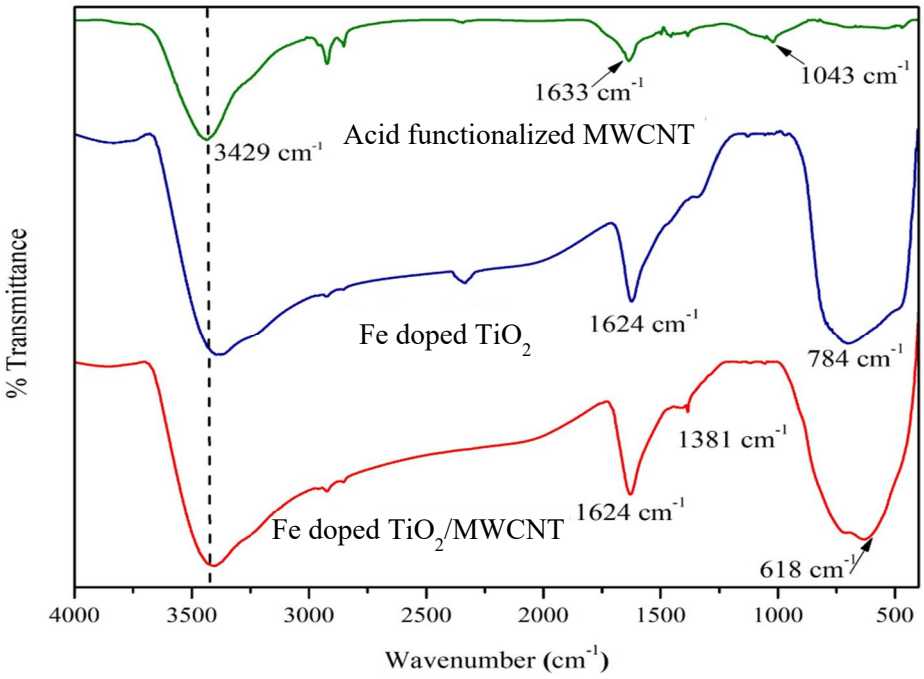

Figure 3.2 FTIR spectra of MWCNT, Fe doped TiO_2 and Fe doped TiO_2/MWCNT.

3.3.3 SEM, EDX and TEM analyses.

Surface morphology of Fe doped TiO_2/MWCNT is presented in **Figure 3.3**. The SEM images in **Figure 3.3 (a) and (b)**, show MWCNTs before and after acid functionalization. After functionalization the length of tubes decreases and the population of the tubes gets increased. Surface modification of MWCNTs is necessary as it introduces various oxygen containing functional groups. These modified MWCNTs can interact with TiO_2 and form bonds *via* carbonyl or carboxyl groups.

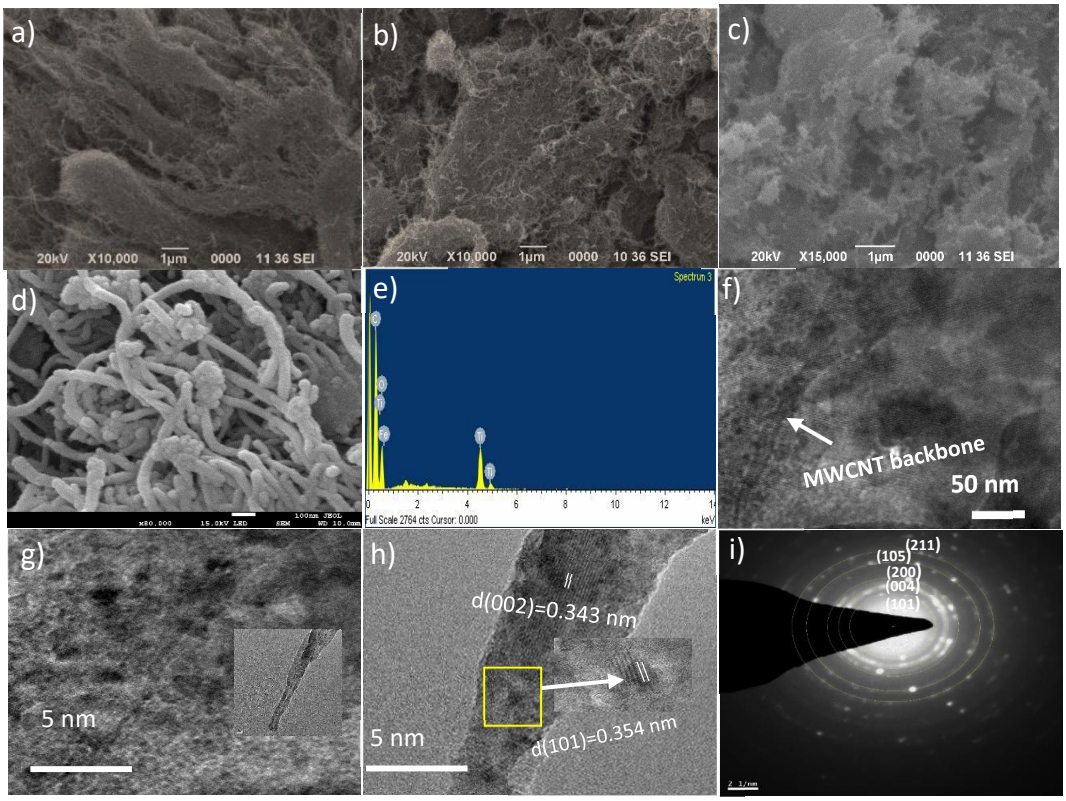

Figure 3.3 SEM images showing surfaces of (a) MWCNT, (b) acid functionalised MWCNT(c,d) Fe doped TiO_2/MWCNT, (e) EDX spectra; (f,g) TEM image showing surface of the composite, the inset of (g) shows a cracked portion of the composite that leds the MWCNT pull out; (h) HRTEM image showing accumulation of metal particles on MWCNT backbone alongwith (002) plane of MWCNT (The inset focused HRTEM shows (101) plane of anatase) and (i) SAED pattern of Fe doped TiO_2/MWCNT.

It has been claimed that interaction between MWCNTs and TiO_2 can lead to formation of new energy level which decreases the band gap [28]. Such an effect is highly beneficial for catalytic applications. **Figure 3.3 (c)** shows a rough surface where Fe doped TiO_2 particles grow on MWCNTs. SEM image with higher resolution in **Figure 3.3 (d)** proclaims that Fe doped TiO_2 particles are dispersed well over MWCNT without free standing particles located away from the support. The EDX spectra in **Figure 3.3 (e)** confirms the presence of C, O, Ti and Fe elements as the expected ratio with minor impurities. Growth of Fe doped TiO_2 particles on the MWCNT backbone was further observed by TEM image in **Figure 3.3 (f)** and **(g)**. In **Figure 3.3 (g)** accumulated particles are clearly visible on the MWCNT rather than agglomeration randomly. The inset TEM in **Figure 3.3 (g)** shows a fractured portion that has propagated through the metal oxide phase and led to the exposure of MWCNT backbone. Strong adhesion between particles and MWCNTs greatly promotes electron transport. The HRTEM image of Fe doped TiO_2/MWCNT, **Figure 3.3 (h)** shows the distance between lattice fringes by 0.343 nm that represents the (002) plane of MWCNT and the inset focused HRTEM in **Figure 3.3 (h)** exhibits a d spacing of 0.354 nm, representing the significant (101) crystal plane of anatase phase which is well agreed with the p-XRD data (**Figure 3.1**). Selected area electron diffraction (SAED) Pattern (**Figure 3.3 (i)**), represents well-defined concentric rings that establish the polycrystallinity of the synthesized nanocomposite. The circular rings correspond to the planes of anatase TiO_2: (101), (004), (200), (105), and (211).

3.3.4 Electrocatalytic performance towards HER

Electrocatalytic performance of Fe doped TiO_2/MWCNT composite for HER was examined using a three-electrode set-up in 0.5 M H_2SO_4 solution at ambient temperature. All electrochemical measurements were carried out with the composite that has 0.50 wt% MWCNT. This composition gives the optimum results as will be seen in the following sections. The catalytic performance was measured from the polarization curves (J-V plots) derived from linear sweep voltammetry (LSV) analysis measured at a scan rate of 50 mV sec^{-1}. All the potentials were measured with SCE and then modified to reversible hydrogen electrode (RHE).

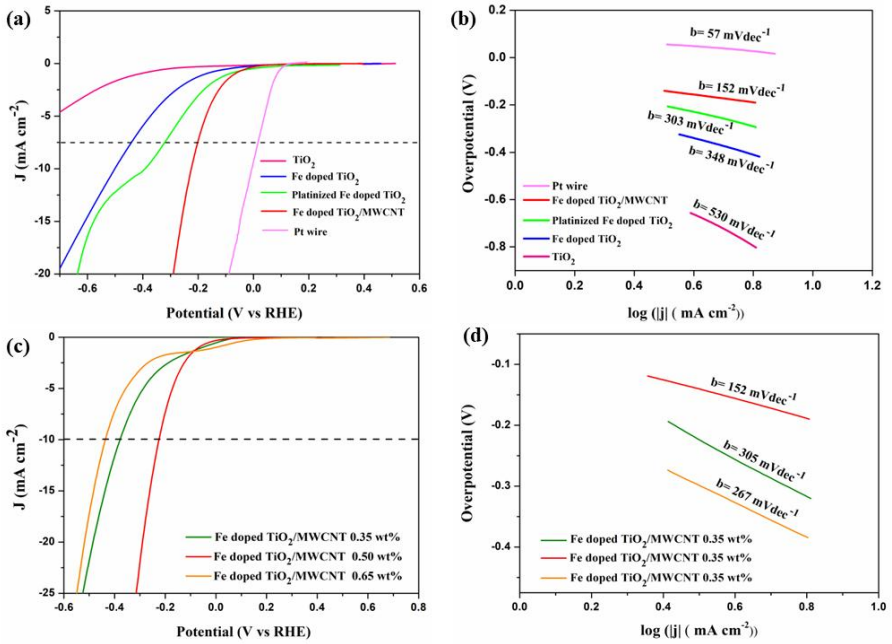

Figure 3.4 Electrocatalytic performances of Pt wire, Fe doped TiO_2/MWCNT, platinized Fe doped TiO_2, Fe doped TiO_2 and bare TiO_2 in terms of their (a) polarization curves and (b) Tafel Plots; Performances of Fe doped TiO_2/MWCNT with varying MWCNT content (wt%=0.65, 0.50, 0.35) in terms of their (c) polarization curves and (d) Tafel plots.

Figure 3.4 (a) shows the voltammograms where the onset potential of Fe doped TiO_2/MWCNT (~115 mV) is compared with that of platinized Fe doped TiO_2 (~140 mV), Fe doped TiO_2 (~230 mV) and TiO_2 (~460 mV). Evidently, it reveals that Fe doped TiO_2/MWCNT shows better activity than the others. The catalytic efficiency is improved far better after incorporating MWCNT in Fe doped TiO_2, where onset potential value becomes comparable to that of Pt electrode, the value of which is ~ 0 V vs RHE. It is significant that integrating Fe doped TiO_2 and MWCNT together increases the HER catalytic performance. The most prominent contribution comes from the presence of MWCNT that causes a decrease in electronic band gap, which is discussed in the next section. Also, percolation phenomenon and already presented free electron in sp^2 hybridised carbon atom in the long tubular structure of MWCNT accounts for the increasing conductivity of the catalyst [29]. The catalyst Fe doped TiO_2/MWCNT drives HER with a smaller overpotential value of 221 mV at current density 10 mA cm^{-2} compared to platinized Fe doped TiO_2 (388 mV at 10 mA cm^{-2}) and Fe doped TiO_2 (504 mV at 10 mA cm^{-2}).

The kinetics of HER was analyzed by tafel slope which was derived by fitting the slope of the polarization curve to the equation 2.2 (a) and (b). HER mechanism can be established from the Tafel slope value that entails the following steps

(1) Volmer: $H^+ + e^- \longrightarrow H_{ads}$

(2) Heyrovsky: $H_{ads} + H^+ + e^- \longrightarrow H_2$

(3) Tafel: $H_{ads} + H_{ads} \longrightarrow H_2$ [30]

Fe doped TiO_2/MWCNT has a Tafel slope value of 152 $mVdec^{-1}$ (**Figure 3.4 (b)**) which ensures that the HER kinetics is proceeded by Volmer-Heyrovsky mechanism and the plausible way of it is as follows

$$H_3O^+(aq) + e^- + A^* \longrightarrow AH_{ads} + H_2O$$

$$AH_{ads} + H_3O^+(aq) + e^- \longrightarrow H_2(g) + H_2O(l) + A^*$$

A* denotes the active catalytic sites of the catalyst and H_{ads} denotes the adsorbed hydrogen on the active sites. It has been reported that a smaller Tafel slope means faster HER rate and smaller energy for the HER [31].

Effect of MWCNT content: The electrocatalytic activity of Fe doped TiO_2/MWCNT catalyst was examined by varying the percentage contents of MWCNT: 0.35, 0.50 and 0.65 wt%. From the polarization curves (**Figure 3.3 (c)**), the catalytic activity shows an increasing trend with increasing MWCNT loading upto 0.50 wt% but upon further increase in MWCNT content, the catalytic efficiency is found to decrease. 0.50 wt% shows the smallest Tafel slope value 152 mV dec^{-1} while 0.65 wt% and 0.35 wt% have Tafel slopes of 267 mV dec^{-1} and 305 mV dec^{-1} respectively (**Figure 3.3 (d)**). Thus, the optimum composition for the best catalytic activity can be considered to be 0.50 wt% of MWCNT. Electronegativity difference between the non-precious metal and carbon leads to the transfer of electrons from metal to carbon when the both interact with each other and this causes the conductivity of MWCNTs to increase [32]. Since electrons are involved in the HER process, the better conductivity makes Fe doped TiO_2/MWCNT with 0.50 wt% MWCNT an ideal catalyst. However, after reaching an optimum composition further increase of MWCNT concentration leads to coverage of the active sites and MWCNTs wall becomes inert to H_{ads} and the catalytic activity further deteriorates. That is why tuning the component concentration is very important so that maximum efficiency can be extracted from it. MWCNTs also has a similar effect on Fe as well. Deng *at al.* used

density functional theory (DFT) simulations to correlate the structure-function relationship between Fe and CNTs [33]. Charge transfer takes place from Fe to C, due to which charge density on MWCNT increases, and the Fermi level of Fe-MWCNTs is lowered in comparison to MWCNTs. Due to this, a stronger C-H interaction is formed on the catalysts' surface which stabilizes the H_{ads} species.

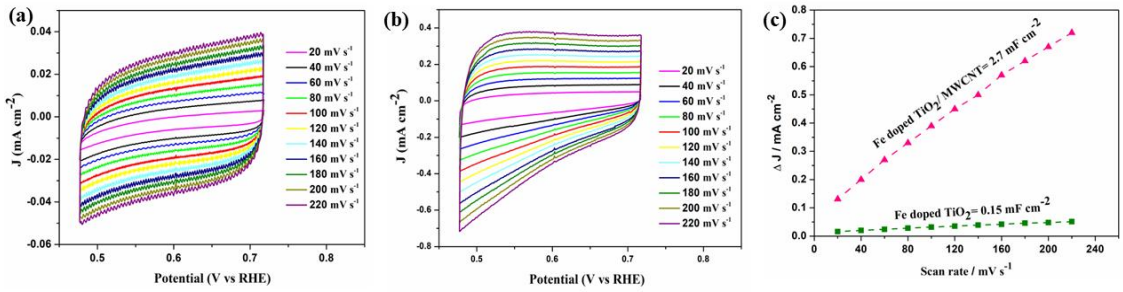

Figure 3.5 Cyclic voltammograms at various scan rate within a non-faradic region for (a) Fe doped TiO_2 and (b) Fe doped TiO_2/MWCNT, (c) charging current density against scan rate (C_{dl} values calculated for Fe doped TiO_2 and Fe doped TiO_2/MWCNT).

Electrochemical active surface area (ECSA) is another feature that has a prominent effect on the electrocatalytic activity. Electrodes with higher ECSA evince higher catalytic activity. Values of ECSA was obtained from the electrochemical double-layer capacitance (C_{dl}) which was analysed under a non-Faradaic region. C_{dl} was acquired by fitting the values of the capacitive current (i) and scanning rate (v) obtained from CV performed (**Figure 3.5 (a)** and **(b)**) in the equation 2.5. C_{dl} values calculated for Fe doped TiO_2/MWCNT and Fe doped TiO_2 are shown in **Figure 3.5 (c)** [34, 35]. Calculated C_{dl} and R_f values for Fe doped TiO_2/MWCNT and Fe doped TiO_2 are as given in Table 3.1. From these values, it can be proposed that MWCNTs have greatly increased the R_f and ECSA. Thus, Fe doped TiO_2/MWCNT recieves an advantage in active surface area (ECSA) and active sites over Fe doped TiO_2 for the improvement of electrocatalytic HER activity.

Table 3.1 Double layer capacitance C_{dl}, roughness factor R_f and electrochemical active surface area **ECSA** values obtained for different catalysts			
Working electrode	C_{dl} (mF cm^{-2})	R_f (cm^{-2})	*ECSA* (cm^2)
Fe doped TiO_2	0.15	7.5	0.525
Fe doped TiO_2/MWCNT	2.7	135	9.45

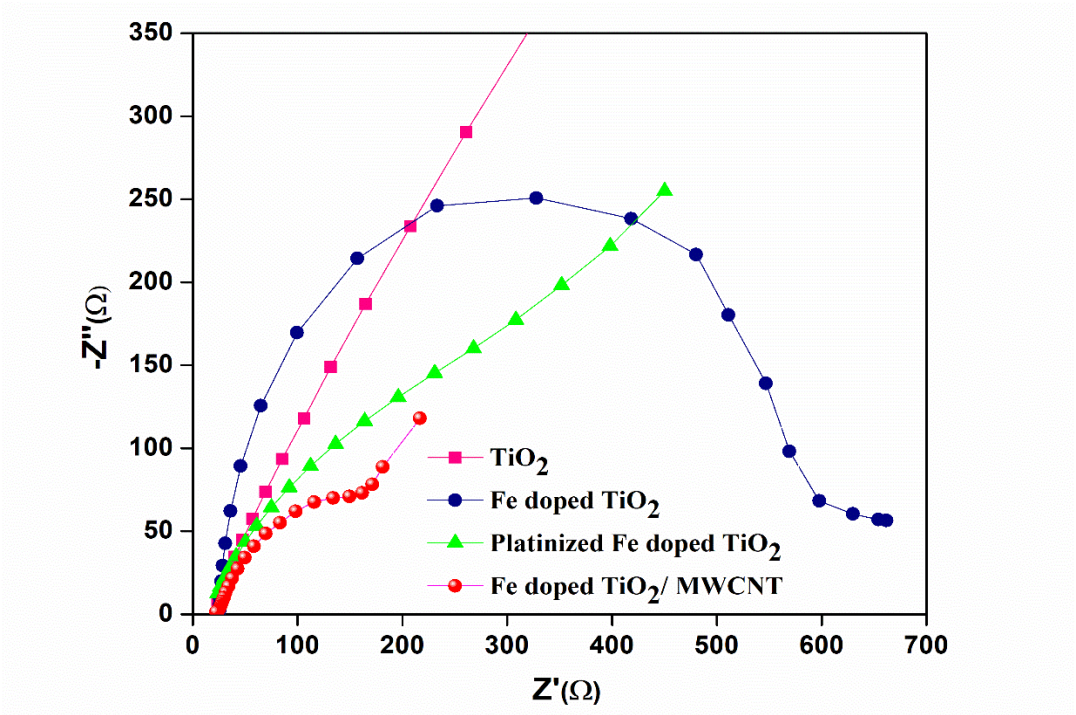

Figure 3.6 Nyquist impedance plots of various catalysts

Electrochemical impedance spectroscopy (EIS) was calibrated at an open circuit voltage, E = 0.3V (vs RHE) in between the frequency range of 100 mHz-10 kHz. In **Figure 3.6**, the Nyquist plots are displayed where the diameter of the semicircles explains the charge-transfer resistance (R_{ct}) of the corresponding catalysts. A smaller diameter denotes a rapid charge transfer process which results better conductivity [36]. The synthesized composite Fe doped TiO_2/MWCNT shows R_{ct} value of 200 Ω which is much smaller as compared to those of platinized Fe doped TiO_2 (~500 Ω), Fe doped TiO_2 (~588 Ω) and TiO_2 (~6500 Ω). This small R_{ct} value of Fe doped TiO_2/MWCNT validates faster HER kinetics. It is evident from the EIS measurements that incorporation of MWCNTs drastically increases the catalytic conductivity.

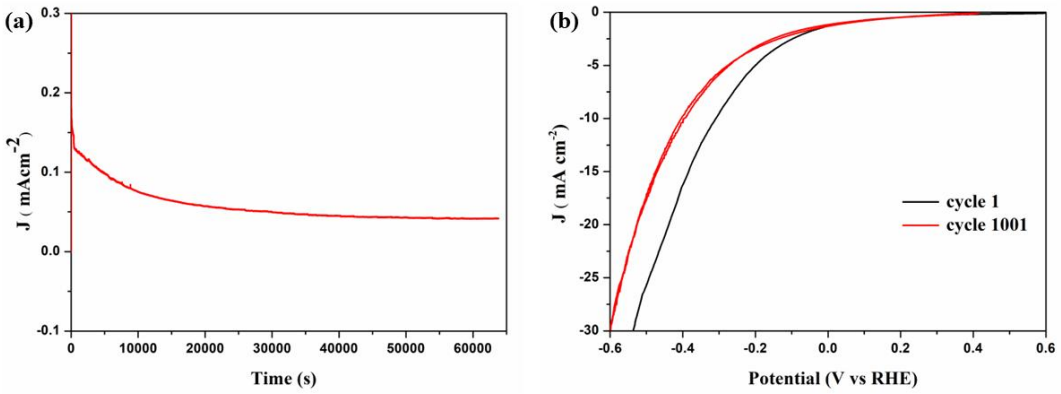

Figure 3.7 Electrochemical stability of Fe doped TiO_2/MWCNT: (a) CV profiles recorded at 20 mV s^{-1} up to 1000 cycles and (b) time dependence study at a static overpotential of 217 mV in 0.5 M H_2SO_4.

Stability of Fe doped TiO_2/MWCNT was probed via performing CV analysis from 0.1 V to −0.54 V (vs RHE) at 20 mV sec^{-1} (**Figure 3.7 (a)**) up to 1000 cycles. The catalyst almost retained its onset potential which gives evidence of the fine stability of the catalyst. But apparently the overpotential at 10 mA cm^{-2} of 1st cycle and 1001 cycle showed a difference though the onset potential remained intact. This may be mainly due to the corrosion of Fe doped TiO_2 particles that are on the surface of MWCNT. MWCNT cannot carry out HER alone as Gibbs free energy of H_{ads} is quite high on CNTs leading to the inertness of MWCNT walls, so upon corrosion of Fe doped TiO_2 nanoparticles charge density in the catalytic surface decreases and so adsorbed H_{ads} becomes unstable leading to the increase of overpotential value with time. Furthermore, durability of the catalyst in acidic aqueous solution was estimated through prolonged electrolysis at a steady overpotential of 217 mV (vs RHE) for 63,809 sec (**Figure 3.7 (b)**). Initial current degradation in the chronoamperometric (CA) graph was observed which was may be due to adsorbance of proton on the catalyst surface and hence takes time to get stability but after that the prolonged stable current density suggesting its excellent durability.

In order to compare the electrocatalytic performance of the synthesized catalyst towards HER in acidic condition with other recently documented precious and non-precious metal-based catalysts, a table is provided (Table 3.2). The activity of our

catalyst is found to be better than most of the mentioned TiO_2 and CNT based catalysts.

Table 3.2 Comparison of activities of different TiO_2 and CNT based catalysts towards HER.

Material	Electrolyte	Loading (mg cm^{-2})	Substrate area (cm^2)	Stability	Over-potential (mV)	Tafel slope (mV dec^{-1})	Ref
WC/CNT	0.05 M H_2SO_4	N/A	0.04	1000 cycles	489	122	[22]
WS_2/CNT	0.05 M H_2SO_4	N/A	0.04	1000 cycles	648	182	[22]
FeCo@NCNTs–NH	0.1 M H_2SO_4	0.32	0.7	10000 cycles	350	74	[23]
$MoSe_2$/rGO/CNT	0.5 M H_2SO_4	N/A	N/A	10000 sec	240	53	[37]
CoS_2 NS/RGO/CNT	0.5 M H_2SO_4	1.15	0.5	500 cycles	142	51	[38]
$Fe_{0.9}Co_{0.1}S_2$/CNT	0.5 M H_2SO_4	0.4	0.25	40 h	120	46	[39]
Pd doped TiO_2	0.5 M H_2SO_4	0.4	0.1256	12 h	430	63	[40]
P-doped CNTs encapsulated nickel hybrids	0.5 M H_2SO_4	N/A	2	20 h	135	81	[41]
Pt–graphitic tube–FeCo/Cu	0.5 M H_2SO_4	N/A	N/A	10000 cycles	18	24	[42]
Mo_2C/CNT-GR	0.5 M H_2SO_4	0.65-0.67	N/A	1000 cycles	250	100	[44]
Fe doped TiO_2/MWCNT	0.5 M H_2SO_4	0.02	0.07	1000 cycles, 17.7 h	221	152	This work

3.4 Conclusion

In summary, this study presents a successful application of eco-friendly and cost-efficient electrocatalyst Fe doped TiO_2 /MWCNTs towards HER. The composite requires a small overpotential of 0.221 V at a current density of 10 mA cm^{-2} with a Tafel slope value of 152 mV dec^{-1}. A range of catalysts with varying wt% of MWCNT loadings were developed, and the best catalytic performance was acquired with 0.50 wt% of MWCNT content. The increased electrocatalytic efficiency towards HER can be solely attributed to the incorporation of MWCNTs which not only provide robust metal-support interactions but also increase surface area and produce sufficient active

sites to perform the reaction efficiently. Moreover, the tubular backbone in the catalyst supports the enhancement of charge density aiding the HER, and offers an affordable and feasible alternate electrocatalyst to replace the expensive Pt electrode.

3.5 References

[1] Kumar, G.M., Ilanchezhiyan, P., Siva, C., Madhankumar, A., Kang, T.W., and Kim, D.Y. Co-Ni based hybrid transition metal oxide nanostructures for cost-effective bi-functional electrocatalytic oxygen and hydrogen evolution reactions. *International Journal of Hydrogen Energy*, *45*(1):391-400, 2020.

[2] Miao, R., Dutta, B., Sahoo, S., He, J., Zhong, W., Cetegen, S.A., Jiang, T., Alpay, S.P., and Suib, S.L. Mesoporous iron sulfide for highly efficient electrocatalytic hydrogen evolution. *Journal of the American Chemical Society*, *139*(39):13604-13607, 2017.

[3] Huang, Z., Chen, Z., Chen, Z., Lv, C., Humphrey, M.G., and Zhang, C. Cobalt phosphide nanorods as an efficient electrocatalyst for the hydrogen evolution reaction. *Nano Energy*, *9*:373-382, 2014.

[4] Chen, W., Qian, G., Xu, Q., Yu, C., Yu, M., Xia, Y., and Yin, S. Efficient bifunctional catalysts for overall water splitting: porous Fe–Mo oxide hybrid nanorods. *Nanoscale*, *12*(13):7116-7123, 2020.

[5] Ingram, D.B. *Composite Silver/Titania Photocatalysts for Visible Light Water Splitting: The Role of Silver Surface Plasmons* (Doctoral dissertation, University of Michigan), 2011.

[6] Ferreira, H.S., Ferreira, H.S., da Silva, M.V., Maria da Graça, C., Bargiela, P., Rangel, M.D.C., Eguiluz, K.I., and Salazar-Banda, G.R. Improved electrocatalytic activity of Pt supported onto Fe-doped TiO_2 toward ethanol oxidation in acid media. *Materials Chemistry and Physics*, *245*:122753, 2020.

[7] Li, S., Yang, H., Ren, R., Ma, J., Jin, J., and Ma, J. Facile fabrication of palladium-ionic liquids-nitrogen-doped graphene nanocomposites as enhanced electro-catalyst for ethanol oxidation. *Journal of Power Sources*, *294*:360-368, 2015.

[8] Khan, M.A., Woo, S.I., and Yang, O.B. Hydrothermally stabilized Fe (III) doped titania active under visible light for water splitting reaction. *International Journal of Hydrogen Energy*, *33*(20):5345-5351, 2008.

[9] Danilov, F.I., Tsurkan, A.V., Vasil'Eva, E.A., and Protsenko, V.S. Electrocatalytic activity of composite Fe/TiO2 electrodeposits for hydrogen evolution reaction in alkaline solutions. *International Journal of Hydrogen Energy*, *41*(18):7363-7372, 2016.

[10] Liu, Y., Szeifert, J.M., Feckl, J.M., Mandlmeier, B., Rathousky, J., Hayden, O., Fattakhova-Rohlfing, D., and Bein, T., Niobium-doped titania nanoparticles: synthesis and assembly into mesoporous films and electrical conductivity. *ACS nano*, *4*(9):5373-5381, 2010.

[11] Deng, J., Ren, P., Deng, D., Yu, L., Yang, F., and Bao, X. Highly active and durable non-precious-metal catalysts encapsulated in carbon nanotubes for hydrogen evolution reaction. *Energy & Environmental Science*, *7*(6):1919-1923, 2014.

[12] Cao, Q., Yu, Q., Connell, D.W., and Yu, G. Titania/carbon nanotube composite (TiO_2/CNT) and its application for removal of organic pollutants. *Clean Technologies and Environmental Policy*, *15*:871-880, 2013.

[13] Zhang, K., Kemp, K.C., and Chandra, V. Homogeneous anchoring of TiO_2 nanoparticles on graphene sheets for waste water treatment. *Materials Letters*, *81*:127-130, 2012.

[14] Koli, V.B., Delekar, S.D., and Pawar, S.H. Photoinactivation of bacteria by using Fe-doped TiO_2-MWCNTs nanocomposites. *Journal of Materials Science: Materials in Medicine*, *27*:1-10, 2016.

[15] Silva, C.G. and Faria, J.L. Photocatalytic Oxidation of Phenolic Compounds by Using a Carbon Nanotube-Titanium Dioxide Composite Catalyst. *ChemSusChem: Chemistry & Sustainability Energy & Materials*, *3*(5):609-618, 2010.

[16] Lin, J.F., Pitkänen, O., Mäklin, J., Puskas, R., Kukovecz, A., Dombovari, A., Toth, G., and Kordas, K. Synthesis of tungsten carbide and tungsten disulfide on vertically aligned multi-walled carbon nanotube forests and their application as non-Pt electrocatalysts for the hydrogen evolution reaction. *Journal of Materials Chemistry A*, *3*(28):14609-14616, 2015.

[17] Cao, J., Zhou, J., Zhang, Y., and Liu, A. X. Clean and facile synthesis strategy of MoS_2 nanosheets grown on multi-wall CNTs for enhanced hydrogen evolution reaction performance, Scientific reports 7(1):1-8, 2017.

[18] Deng, J., Ren, P., Deng, D., Yu, L., Yang, F., and Bao, X. Highly active and durable non-precious-metal catalysts encapsulated in carbon nanotubes for hydrogen evolution reaction. *Energy & Environmental Science*, *7*(6):1919-1923, 2014.

[19] Tavakkoli, M., Kallio, T., Reynaud, O., Nasibulin, A.G., Johans, C., Sainio, J., Jiang, H., Kauppinen, E.I., and Laasonen, K. Single-shell carbon-encapsulated iron nanoparticles: synthesis and high electrocatalytic activity for hydrogen evolution reaction. *Angewandte Chemie International Edition*, *54*(15):4535-4538, 2015.

[20] Dai, K., Zhang, X., Fan, K., Zeng, P., and Peng, T. Multiwalled carbon nanotube-TiO_2 nanocomposite for visible-light-induced photocatalytic hydrogen evolution. *Journal of Nanomaterials*, *2014*:4-4, 2014.

[21] Chae, S.Y., Park, M.K., Lee, S.K., Kim, T.Y., Kim, S.K., and Lee, W.I. Preparation of size-controlled TiO_2 nanoparticles and derivation of optically transparent photocatalytic films. *Chemistry of Materials*, *15*(17):3326-3331, 2003.

[22] Sun, T., Fan, J., Liu, E., Liu, L., Wang, Y., Dai, H., Yang, Y., Hou, W., Hu, X., and Jiang, Z. Fe and Ni co-doped TiO_2 nanoparticles prepared by alcohol-thermal method: Application in hydrogen evolution by water splitting under visible light irradiation. *Powder technology*, *228*:210-218, 2012.

[23] Pan, D., Li, X., and Zhang, A. Platinum assisted by carbon quantum dots for methanol electro-oxidation. *Applied Surface Science*, *427*:715-723, 2018.

[24] Holder, C.F. and Schaak, R.E. Tutorial on powder X-ray diffraction for characterizing nanoscale materials. *Acs Nano*, *13*(7):7359-7365, 2019.

[25] Vinayan, B.P., Nagar, R., Raman, V., Rajalakshmi, N., Dhathathreyan, K.S., and Ramaprabhu, S. Synthesis of graphene-multiwalled carbon nanotubes hybrid nanostructure by strengthened electrostatic interaction and its lithium ion battery application. *Journal of Materials Chemistry*, *22*(19):9949-9956, 2012.

[26] Mombeshora, E.T., Simoyi, R., Nyamori, V.O., and Ndungu, P.G. Multiwalled carbon nanotube-titania nanocomposites: Understanding nano-structural parameters and functionality in dye-sensitized solar cells. *South African Journal of Chemistry*, *68*:153-164, 2015.

[27] Sood, S., Umar, A., Mehta, S.K., and Kansal, S.K. Highly effective Fe-doped TiO_2 nanoparticles photocatalysts for visible-light driven photocatalytic degradation of toxic organic compounds. *Journal of colloid and interface science*, *450*:213-223, 2015.

[28] El-Sayed, B.A., Mohamed, W.A., Galal, H.R., Abd El-Bary, H.M., and Ahmed, M.A. Photocatalytic study of some synthesized MWCNTs/TiO_2 nanocomposites used in the treatment of industrial hazard materials. *Egyptian Journal of Petroleum*, *28*(2):247-252, 2019.

[29] Wang, Y. and Weng, G.J. Electrical conductivity of carbon nanotube-and graphene-based nanocomposites. *Micromechanics and nanomechanics of composite solids*:123-156, 2018.

[30] Lotfi, N., Shahrabi, T., Yaghoubinezhad, Y., and Darband, G.B. Electrodeposition of cedar leaf-like graphene Oxide@ Ni–Cu@ Ni foam electrode as a highly efficient and ultra-stable catalyst for hydrogen evolution reaction. *Electrochimica Acta*, *326*:134949, 2019.

[31] Zhang, W., Cui, L., and Liu, J. Recent advances in cobalt-based electrocatalysts for hydrogen and oxygen evolution reactions. *Journal of Alloys and Compounds*, *821*:153542, 2020.

[32] Ali, A. and Shen, P.K. Nonprecious metal's graphene-supported electrocatalysts for hydrogen evolution reaction: fundamentals to applications. *Carbon Energy*, *2*(1):99-121, 2020.

[33] Deng, J., Ren, P., Deng, D., Yu, L., Yang, F., and Bao, X. Highly active and durable non-precious-metal catalysts encapsulated in carbon nanotubes for hydrogen evolution reaction. *Energy & Environmental Science*, *7*(6):1919-1923, 2014.

[34] El-Sherik, A.M. (2017). *Trends in oil and gas corrosion research and technologies: Production and transmission*. Woodhead Publishing, 926.

[35] Gao, D., Guo, J., Cui, X., Yang, L., Yang, Y., He, H., Xiao, P., and Zhang, Y. Three-dimensional dendritic structures of NiCoMo as efficient electrocatalysts for the hydrogen evolution reaction. *ACS Applied Materials & Interfaces*, *9*(27):22420-22431, 2017.

[36] Wang, K., Zhou, C., Xi, D., Shi, Z., He, C., Xia, H., Liu, G., and Qiao, G. Component-controllable synthesis of Co (SxSe1− x) 2 nanowires supported by carbon fiber paper as high-performance electrode for hydrogen evolution reaction. *Nano Energy*, *18*:1-11, 2015.

[37] Park, G.D., Kim, J.H., Park, S.K., and Kang, Y.C. $MoSe_2$ embedded CNT-reduced graphene oxide composite microsphere with superior sodium ion storage and electrocatalytic hydrogen evolution performances. *ACS Applied Materials & Interfaces*, *9*(12):10673-10683, 2017.

[38] Peng, S., Li, L., Han, X., Sun, W., Srinivasan, M., Mhaisalkar, S.G., Cheng, F., Yan, Q., Chen, J., and Ramakrishna, S. Cobalt sulfide nanosheet/graphene/carbon nanotube nanocomposites as flexible electrodes for hydrogen evolution. *Angewandte Chemie*, *126*(46):12802-12807, 2014.

[39] Wang, D.Y., Gong, M., Chou, H.L., Pan, C.J., Chen, H.A., Wu, Y., Lin, M.C., Guan, M., Yang, J., Chen, C.W., and Wang, Y.L. Highly active and stable hybrid catalyst of cobalt-doped FeS_2 nanosheets–carbon nanotubes for hydrogen evolution reaction. *Journal of the American Chemical Society*, *137*(4):1587-1592, 2015.

[40] Shu, C., Du, H., Pu, W., Yang, C., and Gong, J. Trace amounts of palladium-doped hollow TiO_2 nanosphere as highly efficient electrocatalyst for hydrogen evolution reaction. *International Journal of Hydrogen Energy*, *46*(2):1923-1933, 2021.

[41] Jing, S., Wang, D., Yin, S., Lu, J., Shen, P.K., and Tsiakaras, P. P-doped CNTs encapsulated nickel hybrids with flower-like structure as efficient catalysts for hydrogen evolution reaction. *Electrochimica acta*, *298*:142-149, 2019.

[42] Tiwari, J.N., Sultan, S., Myung, C.W., Yoon, T., Li, N., Ha, M., Harzandi, A.M., Park, H.J., Kim, D.Y., Chandrasekaran, S.S., and Lee, W.G. Multicomponent electrocatalyst with ultralow Pt loading and high hydrogen evolution activity. *Nature Energy*, *3*(9):773-782, 2018.

[43] Theerthagiri, J., Cardoso, E.S., Fortunato, G.V., Casagrande, G.A., Senthilkumar, B., Madhavan, J., and Maia, G. Highly electroactive Ni pyrophosphate/Pt catalyst toward hydrogen evolution reaction. *ACS applied materials & interfaces*, *11*(5):4969-4982, 2019.

[44] Youn, D.H., Han, S., Kim, J.Y., Kim, J.Y., Park, H., Choi, S.H., and Lee, J.S. Highly active and stable hydrogen evolution electrocatalysts based on molybdenum compounds on carbon nanotube–graphene hybrid support. *ACS nano*, *8*(5):5164-5173, 2014.